Relationship between electron-phonon interaction and low-frequency Raman anisotropy in high-mobility organic semiconductors

A. Yu. Sosorev[1], D. Maslennikov[1], I. Yu. Chernyshov[2], D. I. Dominskiy[1], V. V. Bruevich[1], M. V. Vener[2], D. Yu. Paraschuk[1]

[1]Faculty of Physics and International Laser Center, M.V. Lomonosov Moscow State University, Moscow 119991, Russia

[2]Department of Quantum Chemistry, Mendeleev University of Chemical Technology, Miusskaya Square 9, Moscow 125047, Russia

Supporting information

1. Computational and experimental details

Computational

Normal vibrational modes (in Γ-point) were calculated within the harmonic approximation by numerical differentiation of the energy gradient with respect to atomic position.[1] The D2 semiempirical Grimme dispersion correction[2] has practically no impact on the intermolecular distances and the mode character.[3,4]

The transfer integrals J were calculated using home-written code based on dimer projection method (DIPRO).[5] To estimate this quantity for a pair (dimer) of molecules (monomers) m and n, J_{mn}, the wavefunctions of these molecules were approximated by their lowest unoccupied molecular orbitals (LUMOs), φ_m and φ_n. The latter were written in the basis of the dimer molecular orbitals φ_i:

$$J_{mn} = \langle \phi_m | H | \phi_n \rangle = \sum_i \sum_j \langle \phi_m | \phi_i \rangle \langle \phi_i | H | \phi_j \rangle \langle \phi_j | \phi_n \rangle \approx \sum_i \langle \phi_m | \phi_i \rangle E_i \langle \phi_i | \phi_n \rangle \quad \text{(S1)}$$

where E_i are the energies of φ_i. Projections of monomer LUMOs on dimer orbitals, $\langle \phi_m | \phi_i \rangle$ and $\langle \phi_i | \phi_n \rangle$, were calculated from the corresponding coefficients in the basis of atomic orbitals.

Experimental

Crystal growth. After the preliminary evacuation of the fused silica growth tube below 2 10^{-3} mbar, the powdered source material was heated at 170°C, sublimated molecules were transported by the carrier gas (by the flow of 4 sccm) to a lower temperature zone (~150°C), where the crystals grew. The crystal growth time was 20 h. After the growth, the crystals were transferred onto glass substrates.

2. Charge transfer directions in crystalline TCNQ and F_2-TCNQ

Table S1 lists the electron transfer integrals for various Dimers of TCNQ and F_2-TCNQ calculated using Eq. S1 at B3LYP/6-31G(d) level (see Section 1). The molecules constituting the dimers are numbered in accordance with Figure 2a,b of the main text. The relative orientation of the molecules in dimers is illustrated in Figure S1. Figure S2 illustrates the lowest unoccupied molecular orbitals (LUMOs) patterns of TCNQ and F_2-TCNQ single molecules and their selected dimers. Significant LUMO density between the molecules in the dimers illustrates considerable charge delocalization and strong electronic coupling (large J) between them.

Table S1. Electron transfer integrals for TCNQ and F_2-TCNQ crystals

Dimer #	Molecules (m-n)	Transfer integral J_{mn}, meV	
		TCNQ	F_2-TCNQ
1	1-2	60	75
2	1-3	34	54
3	1-4	34	75
4	1-5	15	54
5	1-6	10	12
6	1-7	6	5
7	1-8	0.8	0

TCNQ

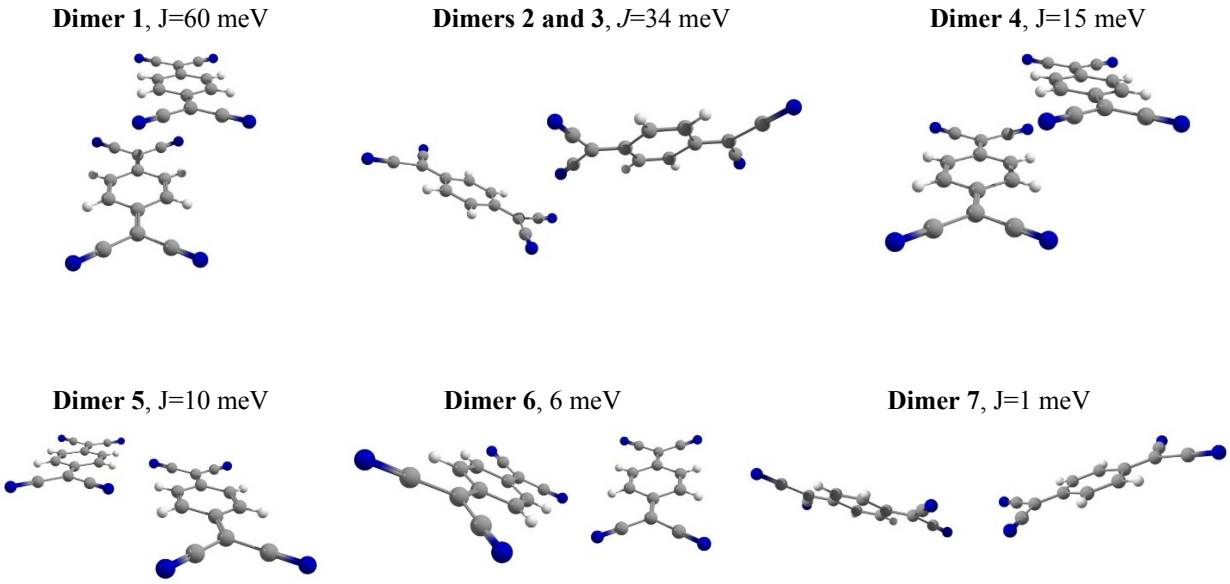

F_2-TCNQ

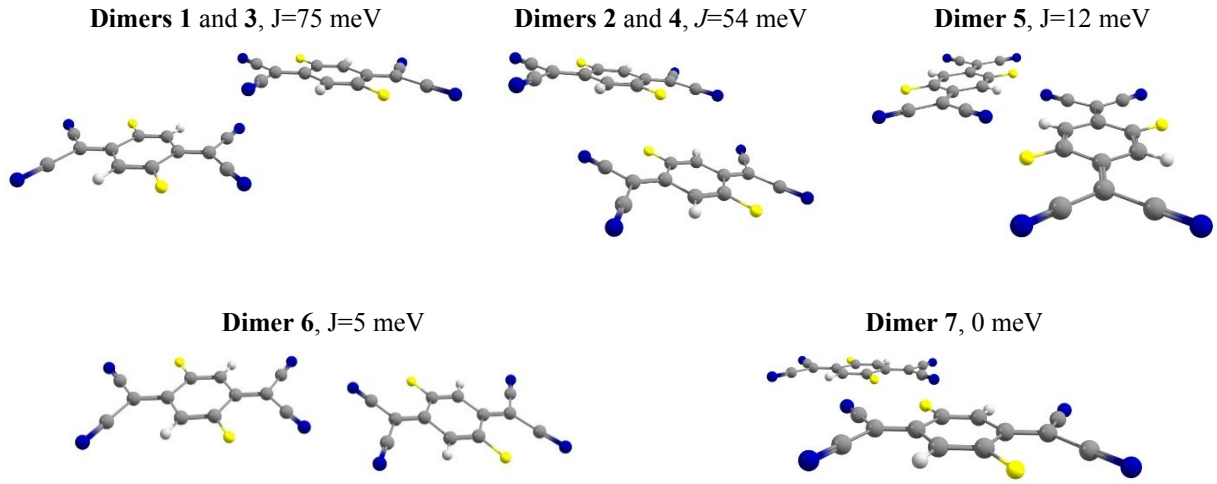

Figure S1. Dimers of TCNQ and F_2-TCNQ from the X-ray data on single crystals.

a) TCNQ

b) F_2-TCNQ

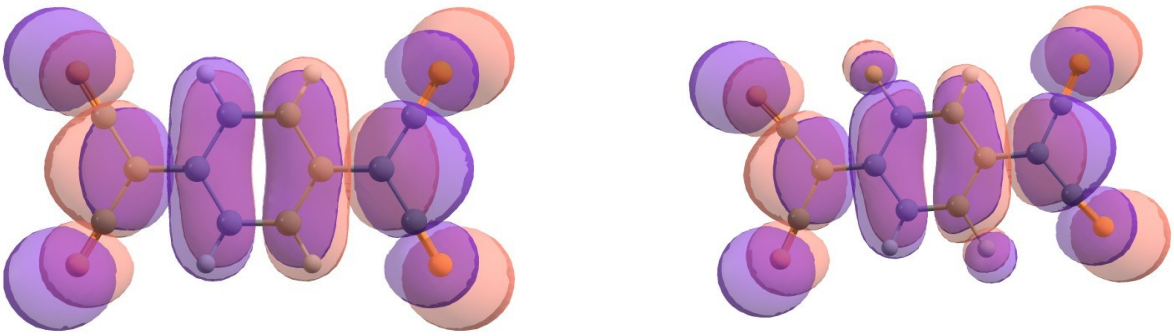

c) TCNQ, Dimer 1

d) F_2-TCNQ, Dimer 1

e) F_2-TCNQ, Dimer 2

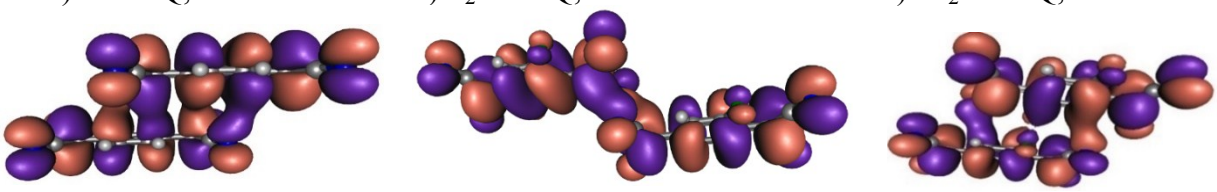

Figure S2. LUMOs of TCNQ (a) and F_2-TCNQ (b) single molecules, Dimer 1 from TCNQ crystal (c), and Dimer 1 (d) and Dimer 2 (e) from F_2-TCNQ crystal.

3. Impact of vibrations on charge transport in TCNQ and F_2-TCNQ

3.1. Overall non-local interaction in Dimer 1 and Dimer 2

Table S2 presents overall estimates of the non-local electron-phonon coupling, $L^{mn} = \sum_i L_i^{mn}$, for Dimers 1 and 2 of TCNQ and F_2-TCNQ. It also shows the variance of the electron transfer integrals along the corresponding directions, σ_J, evaluated from L^{mn} values as[6] $\sigma_J = \sqrt{2L^{mn}kT}$, where k the Boltzman constant and T is the absolute temperature. In the last two columns, the ratio of σ_J to J_{mn} is given. The obtained σ_J / J_{mn} values are in correspondence with those obtained in Ref. [7] using molecular dynamics simulations with classical force field (see Table 2 therein).

Table S2. L^{mn} and σ_J for Dimers 1 and 2 of the TCNQ and F_2-TCNQ crystals.

	L^{mn}, meV		σ_J, meV		σ_J/J_{mn}, meV	
	TCNQ	F_2-TCNQ	TCNQ	F_2-TCNQ	TCNQ	F_2-TCNQ
Dimer 1	10.5	22.5	22.9	33.5	0.38	0.45
Dimer 2	11.8	9.4	24.3	21.7	0.71	0.40

3.2. Vibrational patterns

In crystalline TCNQ, for the charge transfer direction along the Dimer 2 axis, the largest L_i is for the mode at ~42 cm^{-1}. The corresponding vibrational pattern is given in Figure S3a,b. We suggest that large L_i^{13} for this mode stems from its intramolecular part: this mode negligibly affects the distance between the contacting atoms but induces significant changes in the molecular geometry and hence electron density on CN^2 group determining J_{13}. Several other vibrational modes in the range 65-160 cm^{-1} also show significant $L_i^{13} \sim 1$ meV. Considerable number of such modes results from the volatile π-overlapping of the monomers in Dimer 2 (see dotted line in Fig. S3b), which is provided by the contact of just one (N) atom of one monomer with the CN^2 group of the other.

In F_2-TCNQ crystal, charge transfer along the Dimer 2 axis is most affected by the mode at ~ 82 cm^{-1}, which involves significant displacement of the CN^1 moiety with respect to the phenyl ring of the neighboring molecule (Figure S3d). Negligible impact of the latter mode on charge transfer along Dimer 1 axis stems from negligible relative displacement of CN^2 groups (Figure S3c).

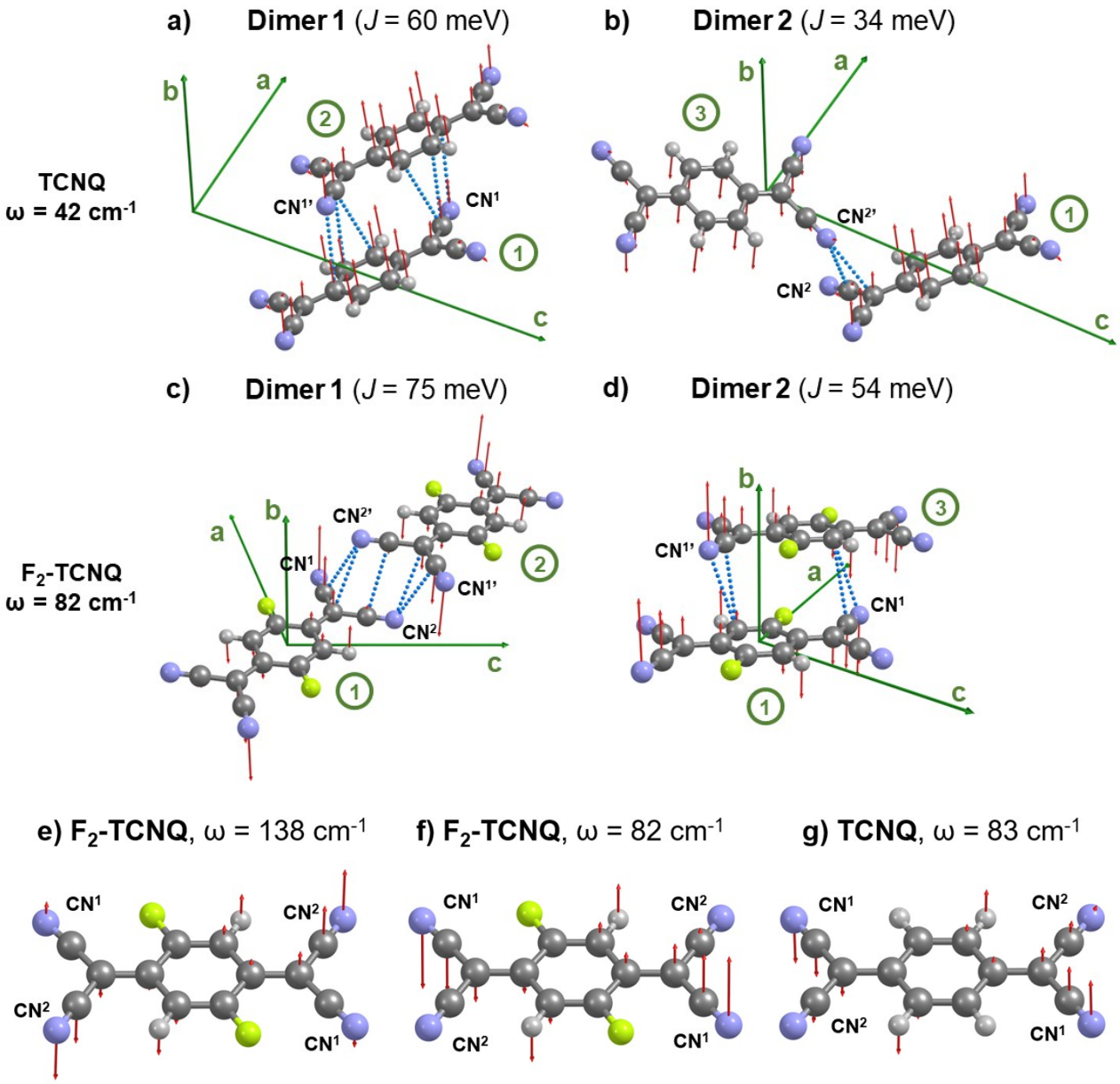

Figure S3. Vibrational patterns of selected modes of crystalline TCNQ and F_2-TCNQ. Atomic displacements for the mode at 42 cm^{-1} in TCNQ crystal (a,b) and 82 cm^{-1} of F_2-TCNQ crystal (c,d) are shown by red arrows within Dimer 1 (left) and Dimer 2 (right). The closest contacts (distances) between the atoms from different monomers (excluding hydrogens) are shown with blue dotted lines. Green arrows depict the crystal axes. Intramolecular vibrational patterns (relative atomic displacements within single molecules) are shown in panels e, f, g for modes at 82 and 138 cm^{-1} of crystalline F_2-TCNQ and for mode 83 cm^{-1} of crystalline TCNQ, respectively.

3.3. Local electron-phonon coupling

Contribution of mode *i* to the local electron-phonon interaction can be estimated as:[8]

$$\lambda_i = \frac{\left(\frac{\partial \varepsilon_m}{\partial Q_i}\right)^2}{2m_i\omega_i^2} \qquad \text{(S2)},$$

where ε_m is the energy of the frontier molecular level (HOMO or LUMO for hole and electron transport, respectively). These contributions for various LF vibrational modes of TCNQ and F_2-TCNQ are shown in Figure S4.

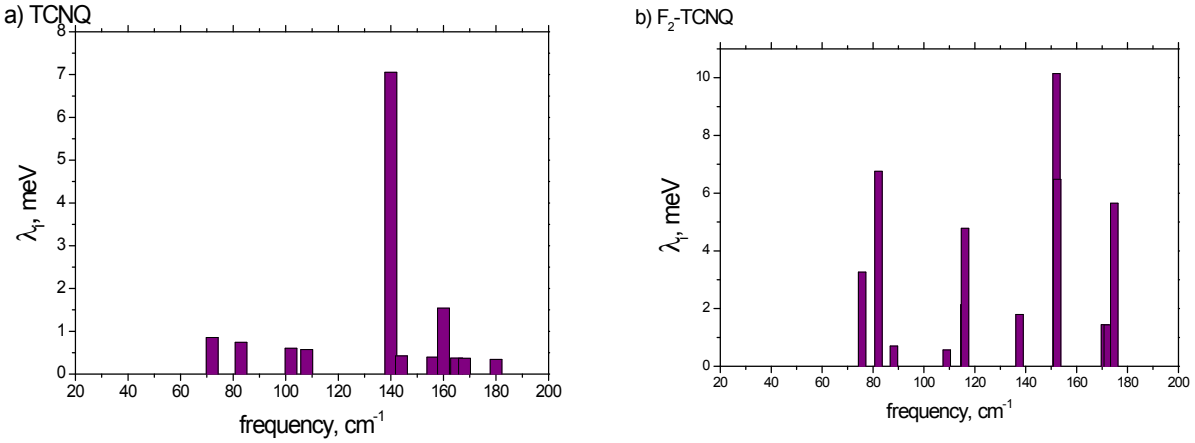

Figure S4. Contribution of various LF vibrational modes to local electron-phonon interaction for TCNQ (a) and F_2-TCNQ (b)

4. Correlation between the Raman anisotropy and contribution to electron-phonon coupling

4.1. Molecular packing in the plane parallel to upper crystal face

Projections of the dimers axes (the straight line linking the centers of the monomers) on the plane of the upper crystal face are important for our analysis of the Raman anisotropy, since the pump laser was polarized in this plane. TCNQ crystal consists of layers, in which molecules are parallel to each other. These layers are parallel to the (001) crystal plane – the upper crystal face in our experiments – as depicted in Figure S5a. In subsequent layers, the molecular packing alternates as shown in Figure S5b,c. As a result, in TCNQ, for a given dimer type (e.g., Dimer 1), projections of the dimers axes from subsequent layers on the upper crystal face are nearly perpendicular as shown in Figure S6a. On the contrary, in F_2-TCNQ, all the molecules are oriented similarly, and thus all dimers of the given type show the same projection on the upper crystal face as shown in Figure S6b.

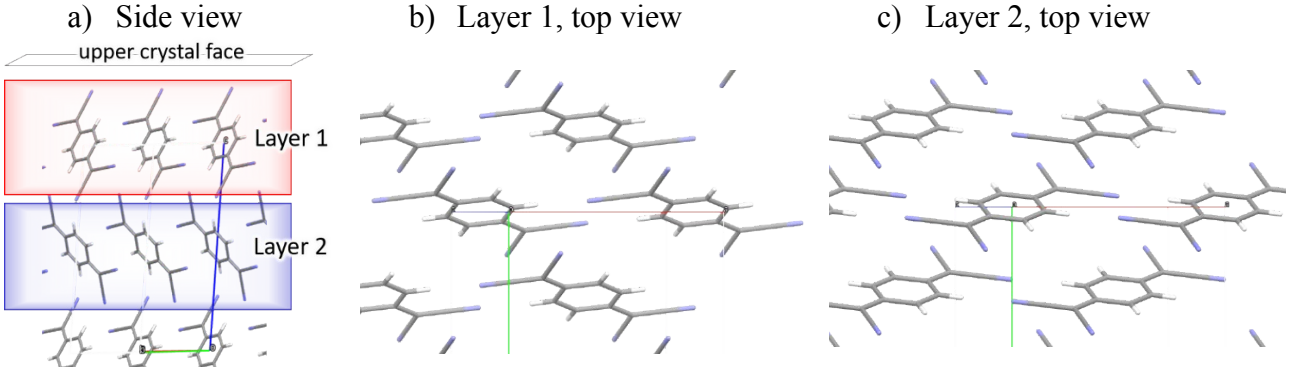

Figure S5. Molecular packing in two subsequent layers of the (001) plane of TCNQ crystal.

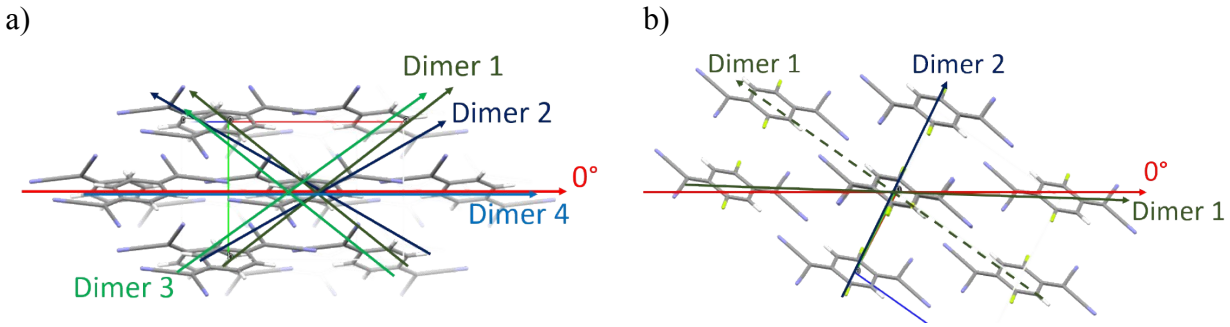

Figure S6. Molecular packing and projections of the dimer axes on the upper face of the investigated crystals (arrows): (001) plane of TCNQ crystal (a) and (110) plane of F_2-TCNQ crystal.

4.2. Raman spectra at different angles and their relation to non-local electron-phonon interaction

In TCNQ and F_2-TCNQ crystals, the relative intensities of the peaks vary with θ (Figure S8). Specifically, for TCNQ, new peaks at ~60, 100 and 145 cm^{-1} emerge for θ=90^0. In F_2-CTNQ, new peaks at ~110 and 170 cm^{-1} arise for θ=90^0. We suggest these peaks were not visible at θ=0^0 since their contribution to *local* electron-phonon interaction is negligible (Figure S4); their emergence at 90^0 can be explained by the contribution to *non-local* electron-phonon interaction (Figure 2b), and local electron-phonon interaction does not obscure them in the latter direction.

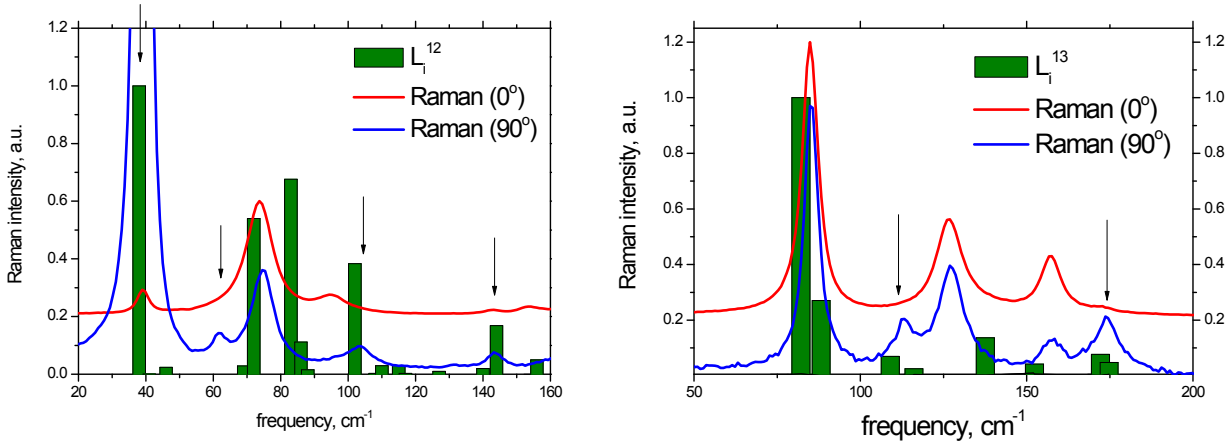

Figure S7. Correlation between the experimental Raman spectra (lines) and calculated contributions of vibrational modes to non-local electron-phonon coupling (bars) for TCNQ (left) and F_2-TCNQ (right). Arrows mark the modes not observed at θ=0° but observed at θ=90°

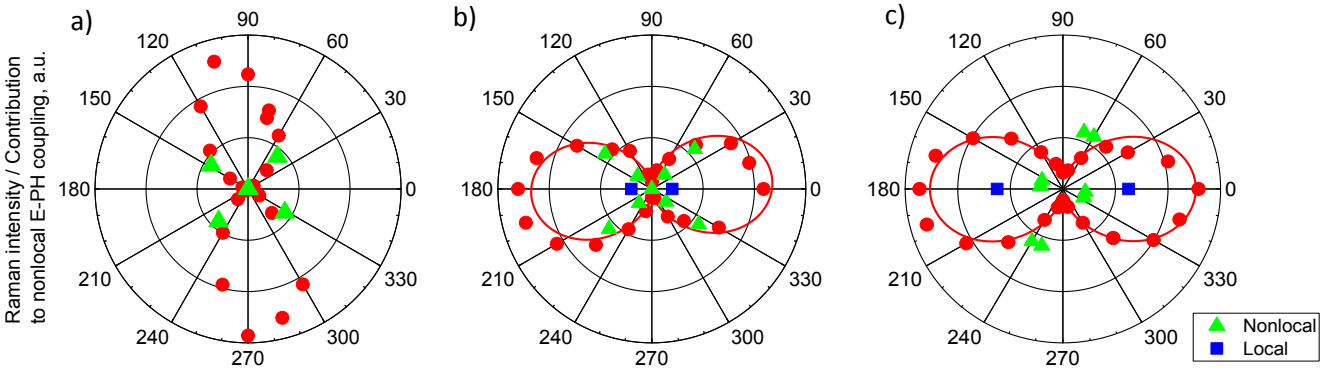

Figure S8. Relationship between Raman anisotropy (circles) and non-local (triangles) and local (squares) electron-phonon coupling. (a) TCNQ, mode at 40 cm^{-1}, (b) TCNQ, mode at 75 cm^{-1} and (c) F_2-TCNQ mode at 78.5 cm^{-1}.

In TCNQ, the mode at ~40 cm^{-1} contributes only to non-local electron-phonon interaction, while the mode at 75 cm^{-1} contributes both to the local and non-local ones (cf. Figures 2 and S4). The mode at ~78.5 cm^{-1} of F_2-TCNQ also contributes both to the local and non-local interaction. Accordingly, for the former mode, there is clear correlation between the Raman anisotropy and L_i^{mn}. On the contrary, for the latter two modes, local electron-phonon interaction obscures this correlation: its contribution to the Raman signal appears to be much larger than for the non-local one. Nevertheless, it is clearly seen that the intensities of the discussed modes are not negligible for θ=90°, where we do not expect

the Raman signal from local electron-phonon coupling. We thus attribute the Raman signal from these modes at θ=90° to their contribution to non-local electron-phonon coupling, in line with Figure S7.

References

1. Dovesi, R.; Saunders, V. R.; Roetti, C.; Orlando, R.; Zicovich-Wilson, C. M.; Pascale, F.; Civalleri, B.; Doll, K.; Harrison, N. M.; Bush, I. J.; D'Arco, P.; Llunell, M. *CRYSTAL09 User's Manual*; University of Torino: Torino, 2009.

2. Grimme, S. Semiempirical GGA-type density functional constructed with a long-range dispersion correction. *J. Comput. Chem.* **2006**, *27*, 1787–1799.

3. Vener, M. V.; Medvedev, A. G.; Churakov, A. V.; Prikhodchenko, P. V.; Tripol'skaya, T. A.; Lev, O. H-Bond Network in Amino Acid Cocrystals with H_2O or H_2O_2. The DFT Study of Serine–H_2O and Serine–H_2O_2. *J. Phys. Chem. A* **2011**, *115*, 13657−13663.

4. Katsyuba, S. A.; Vener, M. V.; Zvereva, E. E.; Fei, Z.; Scopelliti, R.; Laurenczy, G.; Yan, N.; Paunescu, E.; Dyson, P. J. How Strong Is Hydrogen Bonding in Ionic Liquids? Combined X-ray Crystallographic, Infrared/Raman Spectroscopic, and Density Functional Theory Study. *J. Phys. Chem. B* **2013**, *117*, 9094−9105.

5. B. Baumeier, J. Kirkpatrick, D. Andrienko, Phys. Chem. Chem. Phys., 2010, 12, 11103.

6. Y. Li, V. Coropceanu, J.-L. Brédas, in The WSPC Reference on Organic Electronics: Organic Semiconductors (Eds. J.-L. Brédas, S. R. Marder), World Scientific: Singapore, 2016; pp. 193–230.

7. L.-F. Ji, J.-X. Fan, S.-F. Zhanga, A.-M. Ren, *Phys. Chem. Chem. Phys*., 2018, 20, 3784.

8. V. Coropceanu, J. Cornil, D. A. da Silva Filho, Y. Olivier, R. Silbey, J.-L. Brédas, Chem. Rev., 2007, 107, 926.